PCCP

ROYAL SOCIETY OF CHEMISTRY

PAPER

View Article Online
View Journal | View Issue

Cite this: *Phys. Chem. Chem. Phys.*, 2024, **26**, 19130

Computational design of boron-free triangular molecules with inverted singlet–triplet energy gap†

Magdalena W. Duszka, Michał F. Rode and Andrzej L. Sobolewski *

Received 23rd April 2024,
Accepted 28th June 2024

DOI: 10.1039/d4cp01658k

rsc.li/pccp

A novel, computationally designed, class of triangular-shape organic molecules with an inverted singlet–triplet (IST) energy gap is investigated with *ab initio* electronic structure methods. The considered molecular systems are cyclic oligomers and their common feature is electronic conjugation along the molecular rim. Vertical excitation energies from the electronic ground state to the lowest singlet and triplet excited states were computed, as well as vertical emission energies from these states to the ground state. The results underscore the significance of optimizing excited-state geometries to accurately describe the optoelectronic properties of IST molecules, in particular with respect to their application in OLEDs.

1. Introduction

Within the domain of molecular physics, Hund's multiplicity rule, stating that triplet excited states should exhibit lower energy levels than their singlet counterparts with identical orbital configuration, has long served as a guiding principle. This fundamental principle has been a reliable rule governing the ordering of excited states in organic molecules and it was assumed that violations of Hund's multiplicity rule in the excited states of organic compounds are exceptionally rare. Recent computational and experimental developments, however, have confirmed the existence of energy inversion of the first singlet (S_1) and triplet (T_1) excited states, known as inverted singlet–triplet (IST) states, in a number of stable closed-shell organic molecules.[1–3]

The significance of organic molecules featuring nearly degenerate or inverted S_1 and T_1 states extends well beyond theoretical chemistry. IST systems are of relevance when transitions from excited singlet states to triplet states are undesirable. This applies mainly to the development of chromophores for organic light-emitting diodes (OLEDs). Many organic chromophores currently under examination for OLED applications exhibit small positive S_1–T_1 energy gaps,[4–7] relying on reverse intersystem crossing (RISC) from T_1 to S_1, resulting in thermally activated delayed fluorescence (TADF) at room temperature.[8,9] The emergence of organic IST chromophores may open the door to a new generation of OLED devices, capitalizing on the potentially intense fluorescence from these inverted S_1 states and unlocking new possibilities in OLED technology.[10–12] Inverted singlet–triplet molecules also are of interest in photocatalysis,[13] for example for the photocatalytic water-splitting process.[14,15]

This resurgence of interest in the inversion of S_1 and T_1 excited-state energies was primarily initiated by the computational chemistry community. In recent years, researchers have explored design strategies for the engineering of IST molecules with theoretical and computational methods,[16–20] and the theoretical predictions were confirmed by spectroscopic measurements.[1,3,21,22] Molecular structures discovered by these explorations were predominantly nitrogen-doped phenalenes, such as cyclazine or heptazine derivatives,[1,2] along with related triangular[17,23] or hexagonal polycyclic aromatic hydrocarbons[24] with boron–nitride cores. In recent studies, also non-phenalene-based organic molecules were investigated, specifically focusing on non-alternant cyclic hydrocarbons.[25–30]

Organic IST systems typically exhibit specific structural features and characteristics which contribute to their unique electronic properties. While the structural aspects may vary, there are four common themes:

1. Conjugated π-systems: IST molecules represent a subclass of polycyclic aromatic systems with electronic conjugation along the molecular edges.

2. Rigid, planar geometry: IST molecules typically possess rigid internal structures built from nitrogen, boron, or boron–nitride insulating lattices.

3. Electron-donating and electron-withdrawing groups: IST molecules often incorporate electron-donating and electron-withdrawing groups or atoms which allows the fine-tuning of their electronic properties.

4. Heavy-atom substituents: The incorporation of heavy atoms, such as sulfur, may increase the spin–orbit coupling in the molecule and may enhance the quantum yield of RISC.

Institute of Physics, Polish Academy of Sciences, Warsaw, Poland.
E-mail: sobola@ifpan.edu.pl

† Electronic supplementary information (ESI) available. See DOI: https://doi.org/10.1039/d4cp01658k

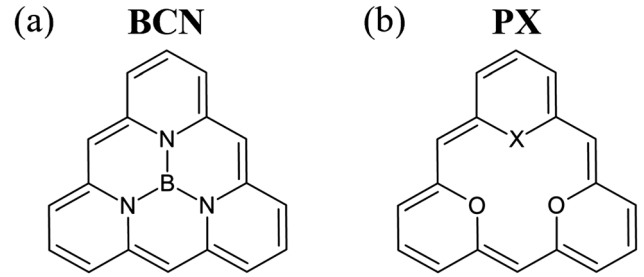

Chart 1 Triangular **BCN** (a) and boron-free (b) molecules (**PX**) considered in this work. X stands for O, NH, or S.

While the concept of organic IST chromophores appears promising, it is crucial to recognize an inherent challenge. Most IST compounds have thus far been found to exhibit minuscule oscillator strengths of the S_1–S_0 transition, resulting in low radiative decay rates.[16,18,19] The long radiative lifetime renders the fluorescence highly susceptible to competing non-radiative decay processes, compromising their emission efficiency.

In this study, we computationally explored the optoelectronic properties of a novel category of boron-free organic IST molecules, which are based on the triangle composed of pyran units (**PX**) as illustrated in Chart 1. Our findings suggest the potential to modify the inherently negative S_1–T_1 energy gap, the wavelength of S_1–S_0 fluorescence, and its intensity through chemical alterations of the parent compounds. The results discussed herein represent a preliminary step towards constructing IST systems based on the **PX** motif.

2. Computational methods

The ground-state equilibrium geometries of all compounds were in a first step optimized using density functional theory (DFT) employing the B3LYP functional,[31,32] augmented with Grimme's D3 dispersion correction.[33] The computation of the Hessian verified that the optimized stationary points represent energy minima. Vertical excitation energies of the lowest singlet and triplet states were computed with the second-order algebraic-diagrammatic construction (ADC(2)) method.[34–36] For consistency with the ADC(2) method employed for the excited-state calculations, the ground-state equilibrium geometries were re-optimized using the Møller–Plesset (MP2) method,[34] with the DFT equilibrium geometries serving as input. The ADC(2) method was also employed to determine the excited state (S_1 and T_1) equilibrium geometries. For all calculations, the correlation-consistent valence double-zeta cc-pVDZ basis set[35] was used. The calculations were performed with the Turbomole 7.3 program package.[36]

Calculations benchmarking the ADC(2) method and the approximate coupled cluster singles and doubles (CC2) method[37] indicate that the accuracies of both methods are very similar.[38–43] Previous studies have established that only methods explicitly including double excitations can accurately reproduce negative singlet–triplet energy gaps.[1,2,38–42] The ADC(2) method chosen for this study represents a pragmatic compromise between accuracy and computational cost.[43,44] For cyclazine and heptazine, both ADC(2) and CC2 slightly overestimate the excitation energies, but provide a reasonably good estimate of the ST energy gap.

3. Results and discussion

3.1. Vertical excitation energies

The ground-state equilibrium geometries of **BCN** and **PX** with X = O (abbreviated **PO** in what follows), possess D_{3h} symmetry, a feature that profoundly influences their electronic properties. The highest occupied molecular orbital (HOMO) and lowest unoccupied molecular orbital (LUMO) of both compounds are doubly degenerate. This orbital degeneracy gives rise to six valence excited states, three singlet states and three triplet states, with spatial symmetries A_1', A_2', and E'.

The vertical excitation energies of these lowest electronic states of the compounds shown in Chart 1 are listed in Table 1. Notably, in the symmetric systems **BCN** and **PO** (D_{3h} symmetry), the lowest excited singlet state is the nondegenerate $^1A_2'$ ($\pi\pi^*$) state. It is interesting to note that the corresponding triplet state ($^3A_2'$) is energetically higher by 0.312 eV in **BCN** and by 0.387 eV in **PO** (negative singlet–triplet splitting). The $^3A_2'$ state is, however, not the lowest triplet state in both molecules, because the singlet–triplet splitting of the E' and A_1' states is

Table 1 Vertical excitation energies E (in electron volts), oscillator strengths (in parentheses) and the S_1–T_1 vertical energy gaps (Δ_{ST}) of the structures in Chart 1, computed at the ADC(2) level. Note that both components of degenerate E' states are included in the table

BCN(D_{3h})		**PO**(D_{3h})		**PNH**(C_{2v})		**PS**(C_s)	
State	E	State	E	State	E	State	E
			Triplet states				
$^3E'$	**1.914**	$^3A_1'$	**1.911**	$^3B_1$	**1.734**	$^3A''$	**1.550**
$^3E'$	**1.914**	$^3E'$	1.937	$^3A_1$	1.941	$^3A'$	1.552
$^3A_1'$	1.934	$^3E'$	1.937	$^3A_1$	2.111	$^3A'$	1.832
$^3A_2'$	1.943	$^3A_2'$	1.984	$^3B_1$	2.371	$^3A''$	2.137
			Singlet states				
$^1A_2'$	**1.631** (0.0)	$^1A_2'$	**1.597** (0.0)	$^1B_1$	**1.620** (0.037)	$^1A''$	**1.446** (0.023)
$^1A_1'$	2.253 (0.0)	$^1A_1'$	2.254 (0.0)	$^1A_1$	2.398 (0.005)	$^1A'$	2.006 (0.017)
$^1E'$	2.370 (0.293)	$^1E'$	2.572 (0.468)	$^1A_1$	2.659 (0.509)	$^1A'$	2.424 (0.400)
$^1E'$	2.370 (0.293)	$^1E'$	2.572 (0.468)	$^1B_1$	2.699 (0.259)	$^1A''$	2.549 (0.458)
Δ_{ST}	**−0.283**	Δ_{ST}	**−0.314**	Δ_{ST}	**−0.114**	Δ_{ST}	**−0.104**

positive and much larger than that of the A_2' states (see Table 1). As a result, the lowest triplet state has E′ symmetry in **BCN**, but A_1' symmetry in **PO**. The D_{3h} symmetry is reduced in asymmetrically substituted molecules, such as **PNH** (X = NH) and **PS** (X = S), which are of C_{2v} and C_s symmetry, respectively. This reduction of symmetry removes the degeneracy of E′ states.

Remarkably, all the species included in Table 1 are IST systems, that is, the S_1–T_1 energy gap, defined as $\Delta_{ST} = E_S - E_T$, is negative, where E_S and E_T are the lowest singlet and lowest triplet state energies. In the symmetric **PO** and **BCN** molecules, the S_0–S_1 transition is symmetry forbidden (oscillator strength $f = 0$). Breaking the trigonal symmetry axis by substituting one of the oxygen atoms of **PO** with a NH group (in **PNH**), or with sulfur (in **PS**), induces a nonzero transition dipole moment. The reduction of the symmetry is also accompanied by a decrease in the magnitude of the negative singlet–triplet energy gap from −0.283 for **BCN** to −0.104 for **PS**.

To gain deeper insights into this phenomenon, Fig. 1 depicts the electron density of molecular orbitals involved in the lowest-energy electronic transitions. The electron densities presented in Fig. 1 were computed assuming equal occupation of both components of the degenerate E′ HOMO and LUMO orbitals in **BCN** and **PO**. Asymmetric substitutions to the **PX** system remove orbital degeneracy, but still, the S_1 state in both (**PNH** and **PS**) molecules, contains comparable contributions from HOMO/LUMO and HOMO−1/LUMO+1 transitions. Thus for the sake of transparency, the assumption of equal occupation of HOMO and HOMO−1 as well as LUMO and LUMO+1 orbitals were used in computation of electron density involved in this electronic transition.

Fig. 1 reveals that the distribution of the electron densities of HOMO and LUMO displays a characteristic pattern which has been found to be typical for IST systems.[18] For the HOMO and, to a lesser extent, for the LUMO, the electronic charge distribution is expelled from the interior of the molecular framework. Instead, it is largely localized on alternating atoms along the rim. This distribution minimizes the exchange integral, which results in a small S_1–T_1 splitting. However, it also reduces the transition dipole moment and thus the oscillator strength of the S_0–S_1 transition. Chemical substitutions that reduce the symmetry, such as those in **PNH** and **PS**, increase the overlap between electron densities. As mentioned earlier, this affects both the S_1–T_1 energy gap and the oscillator strength of the S_0–S_1 transition.

3.2. Effect of additional symmetry reduction by chemical modification

While a negative Δ_{ST} represents an enticing prospect for applications in OLED devices, the low fluorescence intensity of the S_1 state poses a significant drawback. To delve deeper into the impact of symmetry reduction on the photophysical properties of IST molecules, an overview of the computed spectroscopic parameters for four specifically chosen chemically modified **PX** systems is provided in Table 2. Additionally, an extensive selection of chemically modified **PX** systems is presented in the ESI,† offering a broader exploration of the effects of symmetry alteration on their energy level structure.

Table 2 demonstrates that appropriate chemical modifications to the molecular structure can notably enhance the oscillator strength of the S_0–S_1 transition. However, this effect correlates strongly with a reduction in the magnitude of the negative singlet–triplet splitting: the greater the oscillator strength of the transition, the smaller the negative singlet–triplet energy gap. Bearing in mind that the ADC(2) method tends to overestimate this effect,[43,45] it can be concluded that the molecules listed in the table represent TADF systems with exceptionally small positive ST splitting.

The correlation between the oscillator strength and the singlet–triplet energy gap is revealed by the correlation diagram presented in Fig. 2, which showcases three families of **PX** (X = O, NH, S) systems featuring nitrogen substitutions at the molecular rim. Apart from the systems with symmetry-forbidden S_0–S_1 transitions ($f = 0$), a clear overall correlation between f and Δ_{ST} is discernible. On the other hand, the scattering of the symbols in the diagram reveals nuanced

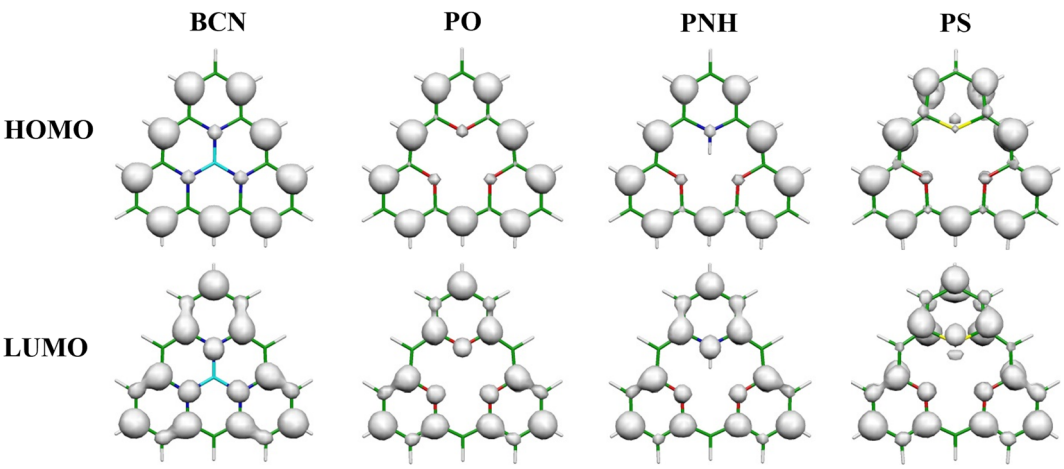

Fig. 1 Electron density of (near)degenerate HOMO and LUMO orbitals of the compounds presented in Chart 1.

Table 2 Vertical excitation energies (in eV) of the lowest excited singlet and triplet states, oscillator strengths for the $S_0 \rightarrow S_1$ transition (in parentheses), and the respective S_1–T_1 energy gap (Δ_{ST}) of selected **PX** molecules, computed at the ADC(2) level of theory

State	**PO-4N**	**PNH-4N**	**PS-2N**	**PNH-2NO$_2$**
	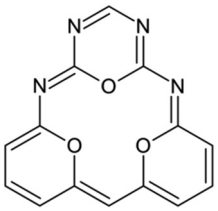	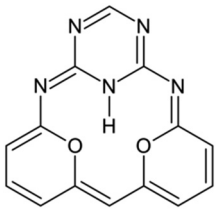	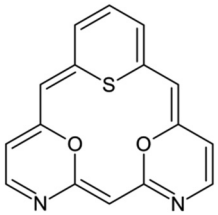	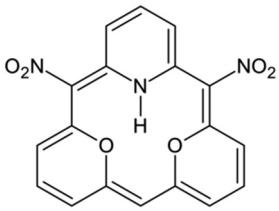
T_1	1.981	1.796	1.623	1.796
S_1	1.953 (0.072)	1.761 (0.086)	1.519 (0.039)	1.792 (0.132)
Δ_{ST}	−0.028	−0.035	−0.104	−0.004

possibilities of manipulating Δ_{ST} and f by molecular symmetry reduction *via* CH/N substitutions at the rim. This variability highlights the flexibility inherent in designing **PX** systems tailored to exhibit specific desired properties, thereby opening up exciting possibilities for manipulating their photophysical functionality. Similar trends have been found for heptazine-based IST compounds.[3,16]

Another intriguing aspect of the computed photophysical properties of the **PX** systems is the correlation between the energy of the S_0–S_1 transition and the number of nitrogen atoms present in the molecular rim. Fig. 3 shows that an increased number of nitrogen atoms raises the energy of the S_0–S_1 transition and enhances the magnitude of the singlet–triplet inversion (for clarity, only nitrogen replacements maintaining the triple symmetry axis of the **PX** system are included in Fig. 3). This observation underscores the intricate relationship between the molecular composition and photophysical properties which can be exploited for the tailored design of OLED chromophores. The impact of the asymmetric CH/N substitutions at the molecular rim on the energy of the S_0–S_1 transition and its oscillator strength is additionally documented in the ESI.†

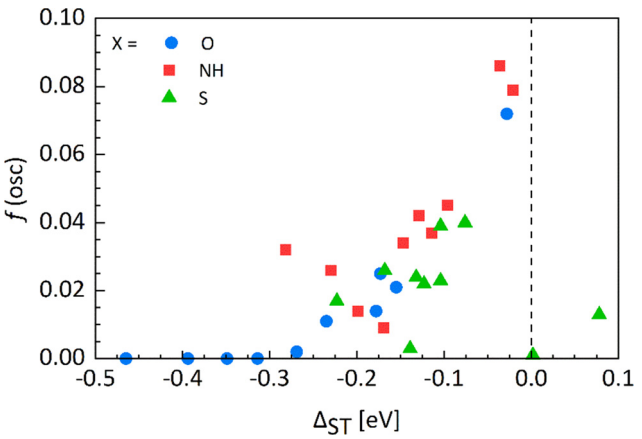

Fig. 2 Correlation between the S_1–T_1 energy gap and the oscillator strength of the $S_0 \rightarrow S_1$ transition for different carbon/nitrogen replacements at the molecular rim (**PO** - blue circles, **PNH** - red squares, **PS** - green triangles), computed at the ADC(2) level (see also Tables S1, S3 and S5 in the ESI†).

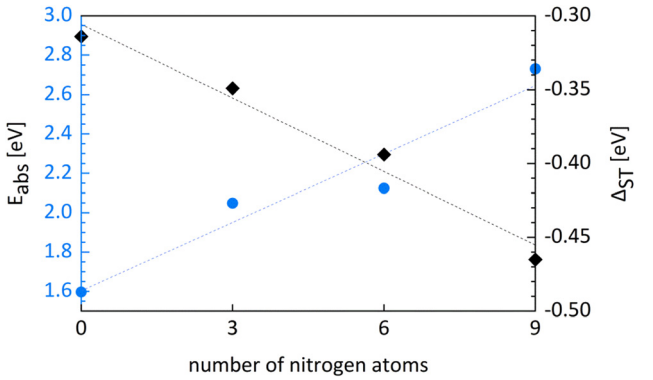

Fig. 3 Correlation between the energy of the S_0–S_1 transition (left axis, blue circles) and the S_1–T_1 energy gap (right axis, black diamonds), plotted against the number of nitrogen atoms present in the molecular rim (molecules **PO**, **PO-3N**, **PO-6N**, **PO-9N** from Table S1 of the ESI†), obtained with the ADC(2) method.

Previous work[19] has established the effect of substitution sites of donors and acceptors on the oscillator strength and the ST energy gap of heptazine derivatives. According to these findings, electron donors attached at atoms which carry electron density in the LUMO orbital preserve the negative energy gap of the molecule, while electron acceptors on the same atoms decrease the gap or even make it positive. Conversely, electron acceptors attached to atoms which carry electron density in the HOMO preserve the negative ST gap, while the gap is reduced by substitution of electron donating groups at these atoms. This rule applies to the molecules considered in the present study (see electron densities in Fig. 1 and in the ESI,† Tables S2, S4 and S6).

3.3. Radiative emission properties

The spectral characteristics discussed so far were computed for the ground-state equilibrium geometries of the **PX** systems. However, for the characterization of radiative emissions (fluorescence, delayed fluorescence, and phosphorescence), it is crucial to consider the photophysical properties at the equilibrium geometries of the excited states (S_1 and T_1). The vertical excitation energies in Table 1 show that in the molecules with a three-

fold symmetry axis (**BCN** and **PO**), the lowest excited singlet state $S_1(A_2')$ is well separated from higher excited singlet states. The two lowest excited triplet states ($^3A_1'$ and $^3E'$), on the other hand, are nearly degenerate. While geometry optimization of the non-degenerate singlet state maintains D_{3h} symmetry, the potential-energy surface (PES) of the degenerate (E′) state may exhibit symmetry breaking due to the Jahn–Teller (JT) effect.

In the ADC(2) method as currently implemented in the TURBOMOLE package, the exploitation of symmetry is limited to Abelian symmetry groups. The highest Abelian subgroup of D_{3h} is C_{2v}. In C_{2v} symmetry, the A_2' symmetry representation becomes B_1, and the two degenerate components of the E′ representation transform as A_1 and B_1, respectively. While the **BCN** molecule maintains D_{3h} symmetry when optimizing the geometry of the $S_1(B_1)$ state, this symmetry is lost when the geometries of the $^3B_1$ and $^3A_1$ states are optimized. The Hessian computed at these stationary points indicates that the optimized $^3A_1$ state represents a local minimum, while the optimized $^3B_1$ state is a first-order saddle point of the JT-deformed two-dimensional PES of the $^3E'$ state. Its relative energy (0.24 eV) with respect to the minimum of the $^3A_1$ state represents the energy barrier for the so-called pseudo-rotation on the PES of the T_1 state.

A qualitatively similar energy-level scheme is obtained for **PO**. Both schemes are shown in Fig. 4. It is evident that the non-degenerate $S_1(A_2')$ state ($^1B_1$ symmetry in the C_{2v} point group) of both molecules exhibits rigidity, that is, the energy relaxation upon geometry optimization is small (0.040 eV and 0.045 eV, respectively) and does not break molecular symmetry. For the degenerate triplet state $^3E'$, on the contrary, the energy relaxation upon geometry optimization is much more pronounced (0.301 eV and 0.378 eV, respectively). A similarly pronounced relaxation of the energy is also observed in the $^1E'$ state. In both E′ states, this effect is attributed to JT-induced geometric instability.

Several interesting conclusions emerge from Fig. 4. Particularly noteworthy is the singlet–triplet inversion measured by the vertical energy difference computed at the ground-state equilibrium geometry, which is remarkably large (−0.283 eV for **BCN** and −0.314 eV for **PO**).

However, the corresponding difference between the adiabatic (geometry-optimized) energies of singlet and triplet states, which represents the 0–0 spectroscopic transition energy, is much smaller (−0.022 eV and −0.007 eV, respectively). Furthermore, the difference between the vertical fluorescence (S_1–S_0) and phosphorescence (T_1–S_0) energies, representing the difference of the peak maxima of the fluorescence (E_{fl}) and phosphorescence (E_{ph}) spectra, respectively, becomes positive (0.312 eV and 0.370 eV, respectively).

A comparison of the level schemes of both molecules clearly shows that the removal of the central boron atom from **BCN** and the replacement of the remaining nitrogen atoms by oxygen atoms (**PO**) have a minor effect on the photophysics. Despite the removal of the central skeleton atom, the **PO** molecule exhibits rigidity which is similar to **BCN**. The inversion of the vertical singlet and triplet states is strongly tied to the electronic conjugation along the molecular rim.

Replacing one of the oxygen atoms in **PO** with the NH group conserves the number of electrons in the system, but reduces the molecular symmetry to C_{2v} or lower. The relevant energy-level schemes for **PNH-4N** (Table 2) and **PNH-6N** (Table S3 in the ESI†), where six nitrogen atoms are symmetrically distributed at the corners of pyran units (see ESI†), are shown in Fig. 5. It is evident that geometry optimization of the lowest singlet and triplet states of **PNH-4N** (both having the B_1 symmetry in the C_{2v} group) does not further lower the molecular symmetry and stabilizes both states by nearly the same amount of energy (0.076 eV for the $^1B_1$ state and 0.069 for the $^3B_1$ state). The adiabatic energies of these states are inverted by merely −0.042 eV. The peak energy of phosphorescence is predicted to be only 0.03 eV lower than the peak energy of fluorescence.

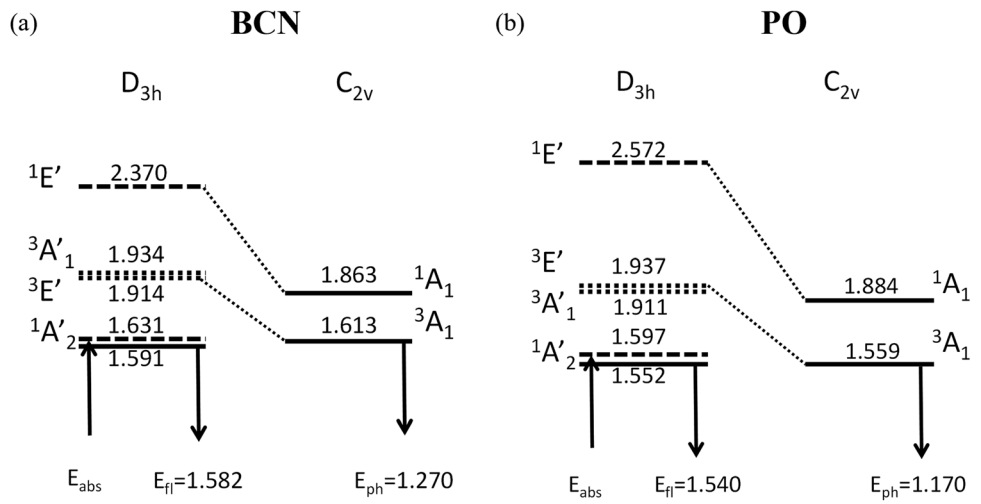

Fig. 4 Energy-level schemes of **BCN** (a) and **PO** (b), determined at the ADC(2) level. Solid lines denote the optimized energy level of the respective electronically excited states, while dashed (dotted) lines denote the vertical energy of the singlet (triplet) states computed at the equilibrium geometry of the electronic ground state. Up and down arrows denote vertical absorption and emission, respectively. Numbers denote energies in electron volts.

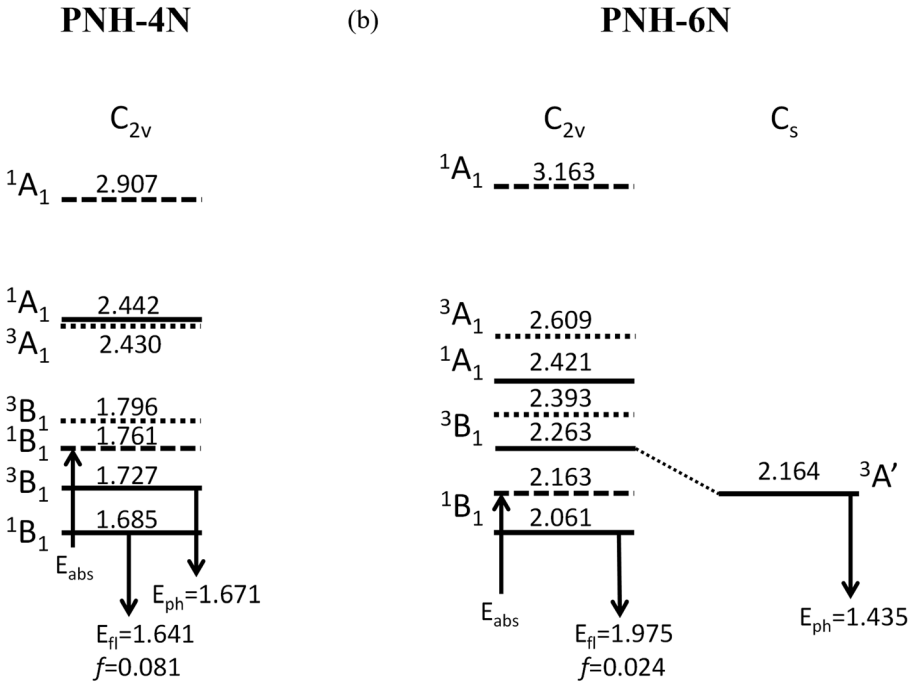

Fig. 5 Energy-level schemes of **PNH-4N** (a) and **PNH-6N** (b) molecules determined at the ADC(2) level. Solid lines denote the optimized energy levels of the respective electronically excited states, and dashed (dotted) lines denote the vertical energy of the singlet (triplet) states computed at the equilibrium geometry of the ground state. Up and down arrows denote vertical absorption and emission, respectively. Numbers denote energy in electronvolts.

The symmetric distribution of six nitrogen atoms along the molecular rim of the **PNH** molecule (**PNH-6N**) maintains C_{2v} symmetry, but notably decreases the energy gap between the $^3B_1$ and $^3A_1$ states (Fig. 5b). While unconstrained geometry optimization of the lowest excited singlet state conserves C_{2v} symmetry, the optimization of the lowest triplet state results in symmetry lowering to C_s (only the molecular plane is conserved). The magnitude of the negative S_1–T_1 vertical energy gap (−0.230 eV) decreases to −0.103 eV for the adiabatic energies. The difference of the emission maxima from these states becomes positive (0.540 eV). Inspection of the equilibrium geometry of the $^3A'$ state (Table S7 of the ESI†) reveals that, apart from the JT distortion, a significant amount of single-double CC bond alternation occurs.

4. Summary

Pyran-substituted triangular aromatic hydrocarbons represent a new category of molecular systems that can be tailored to exhibit robustly negative singlet–triplet energy gaps. The results of this computational study confirm that previously discussed triangular carbon nitrides and triangular boron carbon nitrides are not the only stable organic molecules capable of displaying S_1–T_1 inversion.

A common feature of these IST systems is the electronic conjugation along the outer rim. This effect can be achieved by either filling the interior of an aromatic arene or azaarene molecule with an insulating motif (such as boron nitride) or by removing the central atom(s) altogether, as in the systems examined in this study. The triangular molecules investigated in this work can be considered as cyclic oligomers composed of the pyran units and its derivatives. This finding paves a new path for constructing IST systems utilizing organic molecular units.

In the computational literature the vertical energy gap between the S_1 and T_1 states, computed at the equilibrium geometry of the ground state, is taken as the definition of the ST gap. However, with respect to photophysical processes occurring in and between these states, such as intersystem crossing (ISC) and reverse-ISC (RISC), the adiabatic energies of these states are significant. The adiabatic energies determine the 0–0 line in the fluorescence and phosphorescence spectra.

Data availability

The data supporting this article have been included as part of the ESI.†

Conflicts of interest

There are no conflicts to declare.

Acknowledgements

The Authors would like to thank Wolfgang Domcke for fruitful discussions during the preparation of the manuscript. This research was funded by National Science Centre of Poland, grant number: 2020/39/B/ST4/01723. We gratefully acknowledge Polish high-performance computing infrastructure PLGrid (HPC

Center: ACK Cyfronet AGH) for providing computer facilities and support within computational grant no. PLG/2024/017058.

References

1 J. Ehrmaier, E. J. Rabe, S. R. Pristash, K. L. Corp, C. W. Schlenker, A. L. Sobolewski and W. Domcke, Singlet-Triplet Inversion in Heptazine and in Polymeric Carbon Nitrides, *J. Phys. Chem. A*, 2019, **123**, 8099–8108.

2 P. De Silva, Inverted Singlet-Triplet Gaps and Their Relevance to Thermally Activated Delayed Fluorescence, *J. Phys. Chem. Lett.*, 2019, **10**, 5674–5679.

3 N. Aizawa, Y. J. Pu, Y. Harabuchi, A. Nihonyanagi, R. Ibuka, H. Inuzuka, B. Dhara, Y. Koyama, K.-I. Nakayama, S. Maeda, F. Araoka and D. Miyajima, Delayed fluorescence from inverted singlet and triplet excited states, *Nature*, 2022, **609**, 502–506.

4 F. B. Dias, T. J. Penfold and A. P. Monkman, Photophysics of thermally activated delayed fluorescence molecules, *Methods Appl. Fluoresc.*, 2017, **5**, 012001.

5 X.-K. Chen, D. Kim and J.-L. Brédas, Thermally Activated Delayed Fluorescence (TADF) Path toward Efficient Electroluminescence in Purely Organic Materials: Molecular Level Insight, *Acc. Chem. Res.*, 2018, **51**, 2215–2224.

6 M. A. Bryden and E. Zysman-Colman, Organic thermally activated delayed fluorescence (TADF) compounds used in photocatalysis, *Chem. Soc. Rev.*, 2021, **50**, 7587–7680.

7 H. J. Kim and T. Yasuda, Narrowband Emissive Thermally Activated Delayed Fluorescence Materials, *Adv. Opt. Mater.*, 2022, **10**, 2201714.

8 H. Uoyama, K. Goushi, K. Shizu, H. Nomura and C. Adachi, Highly efficient organic light-emitting diodes from delayed fluorescence, *Nature*, 2012, **492**, 234–238.

9 K. Goushi, K. Yoshida, K. Sato and C. Adachi, Organic light-emitting diodes employing efficient reverse intersystem crossing for triplet-to-singlet state conversion, *Nat. Photonics*, 2012, **6**, 253–258.

10 J. Li, T. Nakagawa, J. Macdonald, Q. Zhang, H. Nomura, H. Miyazaki and C. Adachi, Highly efficient organic light-emitting diode based on a hidden thermally activated delayed fluorescence channel in a heptazine derivative, *Adv. Mater.*, 2013, **25**, 3319–3323.

11 A. L. Sobolewski and W. Domcke, Are Heptazine-Based Organic Light-Emitting Diode Chromophores Thermally Activated Delayed Fluorescence or Inverted Singlet−Triplet Systems?, *J. Phys. Chem. Lett.*, 2021, **12**, 6852–6860.

12 T. Won, K. Nakayama and N. Aizawa, Inverted singlet–triplet emitters for organic light-emitting diodes, *Chem. Phys. Rev.*, 2023, **4**, 021310.

13 A. Actis, M. Melchionna, G. Filippini, P. Fornasiero, M. Prato, M. Chiesa and E. Salvadori, Singlet-Triplet Energy Inversion in Carbon Nitride Photocatalysts, *Angew. Chem., Int. Ed.*, 2023, **62**, e202313540.

14 J. Ehrmaier, X. Huang, E. J. Rabe, K. L. Corp, C. W. Schlenker, A. L. Sobolewski and W. Domcke, Molecular Design of Heptazine-Based Photocatalysts: Effect of Substituents on Photocatalytic Efficiency and Photostability, *J. Phys. Chem. A*, 2020, **124**, 3698–3710.

15 K. Curtis, C. King and S. O. Odoh, Novel Triangulenes: Computational Investigations of Energy Thresholds for Photocatalytic Water Splitting, *ChemPhysChem*, 2023, **24**, e202300556.

16 R. Pollice, P. Friederich, C. Lavigne, G. dos P. Gomes and A. Aspuru-Guzik, Organic molecules with inverted gaps between first excited singlet and triplet states and appreciable fluorescence rates, *Matter.*, 2021, **4**, 1654–1682.

17 J. Sanz-Rodrigo, G. Ricci, Y. Olivier and J. C. Sancho-García, Negative Singlet-Triplet Excitation Energy Gap in Triangle-Shaped Molecular Emitters for Efficient Triplet Harvesting, *J. Phys. Chem. A*, 2021, **125**, 513–522.

18 L. Tučková, M. Straka, R. R. Valiev and D. Sundholm, On the origin of the inverted singlet–triplet gap of the 5th generation light-emitting molecules, *Phys. Chem. Chem. Phys.*, 2022, **24**, 18713–18721.

19 G. Ricci, J.-C. Sancho-García and Y. Olivier, Establishing design strategies for emissive materials with an inverted singlet–triplet energy gap (INVEST): a computational perspective on how symmetry rules the interplay between triplet harvesting and light emission, *J. Mater. Chem. C*, 2022, **10**, 12680–12698.

20 H. Kim, G. D. Scholes and S. K. Min, Extension of molecules with an inverted singlet–triplet gap with conjugated branches to alter the oscillator strength, *Phys. Chem. Chem. Phys.*, 2024, **26**, 5508–5516.

21 J. Li, Z. Li, H. Liu, H. Gong, J. Zhang, X. Li, Y. Wang and Q. Guo, Down-conversion-induced delayed fluorescence via an inverted singlet-triplet channel, *Dyes Pigm.*, 2022, **203**, 110366.

22 D. Blasco, R. T. Nasibullin, R. R. Valiev, M. Monge, J. M. López-de-Luzuriaga and D. Sundholm, Experimental and computational studies of the optical properties of 2,5,8-tris(phenylthiolato)heptazine with an inverted singlet–triplet gap, *Phys. Chem. Chem. Phys.*, 2024, **26**, 5922–5931.

23 S. Pios, X. Huang, A. L. Sobolewski and W. Domcke, Triangular boron carbon nitrides: an unexplored family of chromophores with unique properties for photocatalysis and optoelectronics, *Phys. Chem. Chem. Phys.*, 2021, **23**, 12968–12975.

24 A. L. Sobolewski and W. Domcke, Excited-state singlet–triplet inversion in hexagonal aromatic and heteroaromatic compounds, *Phys. Chem. Chem. Phys.*, 2023, **25**, 21875–21882.

25 D. Casanova, Y. Olivier, J. C. Sancho-García, M. E. Sandoval-Salinas, G. Ricci, A. J. Pérez-Jiménez and J. C. Sancho-Garcí, Correlation *vs*. exchange competition drives the singlet–triplet excited-state inversion in non-alternant hydrocarbons, *Phys. Chem. Chem. Phys.*, 2023, **25**, 26417–26428.

26 Ö. M. H. Omar, X. Xie, A. Troisi and D. Padula, Identification of Unknown Inverted Singlet−Triplet Cores by High-Throughput Virtual Screening, *J. Am. Chem. Soc.*, 2023, **145**, 19790–19799.

27 M. H. Garner, J. T. Blaskovits and C. Corminboeuf, Enhanced inverted singlet–triplet gaps in azaphenalenes and non-alternant hydrocarbons, *Chem. Commun.*, 2024, **60**, 2070–2073.
28 R. Pollice, B. Ding and A. Aspuru-Guzik, Rational Design of Organic Molecules with Inverted Gaps between First Excited Singlet and Triplet, *Matter*, 2024, **7**, 1161–1186.
29 K. Jorner, R. Pollice, C. Lavigne and A. Aspuru-Guzik, Ultrafast Computational Screening of Molecules with Inverted Singlet–Triplet Energy Gaps Using the Pariser–Parr–Pople Semiempirical Quantum Chemistry Method, *J. Phys. Chem. A*, 2024, **128**, 2445–2456.
30 M. H. Garner, J. T. Blaskovits and C. Corminboeuf, Double-bond delocalization in non-alternant hydrocarbons induces inverted singlet–triplet gaps, *Chem. Sci.*, 2023, **14**, 10458–10466.
31 A. D. Becke, Density-functional thermochemistry. III. The role of exact exchange, *J. Chem. Phys.*, 1993, **98**, 5648–5652.
32 C. Lee, W. Yang and R. G. Parr, Development of the Colle-Salvetti correlation-energy formula into a functional of the electron density, *Phys. Rev. B: Condens. Matter Mater. Phys.*, 1988, **37**, 785–789.
33 S. Grimme, J. Antony, S. Ehrlich and H. Krieg, A consistent and accurate ab initio parametrization of density functional dispersion correction (DFT-D) for the 94 elements H-Pu, *J. Chem. Phys.*, 2010, **132**, 154104.
34 C. Møller and M. S. Plesset, Note on an Approximation Treatment for Many-Electron Systems, *Phys. Rev.*, 1934, **46**, 618.
35 T. H. Dunning Jr., Gaussian basis sets for use in correlated molecular calculations. I. The atoms boron through neon and hydrogen, *J. Chem. Phys.*, 1989, **90**, 1007–1023.
36 *TURBOMOLE V7.3 2018*, a development of University of Karlsruhe and Forschungszentrum Karlsruhe GmbH, 1989–2007, TURBOMOLE GmbH, since 2007; available from **https://www.turbomole.com**.
37 O. Christiansen, H. Koch and P. Jørgensen, The second-order approximate coupled cluster singles and doubles model CC2, *Chem. Phys. Lett.*, 1995, **243**, 409–418.
38 M. Schreiber, M. R. Silva-Junior, S. P. A. Sauer and W. Thiel, Benchmarks for electronically excited states: CASPT2, CC2, CCSD, and CC3, *J. Chem. Phys.*, 2008, **128**, 134110.
39 S. P. A. Sauer, M. Schreiber, M. R. Silva-Junior and W. Thiel, Benchmarks for Electronically Excited States: A Comparison of Noniterative and Iterative Triples Corrections in Linear Response Coupled Cluster Methods: CCSDR(3) versus CC3, *J. Chem. Theory Comput.*, 2009, **5**, 555–564.
40 H. H. Falden, K. R. Falster-Hansen, K. L. Bak, S. Rettrup and S. P. A. Sauer, Benchmarking Second Order Methods for the Calculation of Vertical Electronic Excitation Energies: Valence and Rydberg States in Polycyclic Aromatic Hydrocarbons, *J. Phys. Chem. A*, 2009, **113**, 11995–12012.
41 D. Jacquemin, I. Duchemin and X. Blase, Benchmarking the Bethe–Salpeter Formalism on a Standard Organic Molecular Set, *J. Chem. Theory Comput.*, 2015, **11**, 3290–3304.
42 P.-F. Loos, F. Lipparini, M. Boggio-Pasqua, A. Scemama and D. Jacquemin, A Mountaineering Strategy to Excited States: Highly Accurate Energies and Benchmarks for Medium Sized Molecules, *J. Chem. Theory Comput.*, 2020, **16**, 1711–1741.
43 P.-F. Loos, F. Lipparini and D. Jacquemin, Heptazine, Cyclazine, and Related Compounds: Chemically-Accurate Estimates of the Inverted Singlet–Triplet Gap, *J. Phys. Chem. Lett.*, 2023, **14**, 11069–11075.
44 L. Tuč, M. Straka, R. R. Valiev and D. Sundholm, On the origin of the inverted singlet-triplet gap of the 5th generation light-emitting molecules, *Phys. Chem. Chem. Phys.*, 2022, **24**, 18713.
45 D. Drwal, M. Matousek, P. Golub, A. Tucholska, M. Hapka, J. Brabec, L. Veis and K. Pernal, Role of Spin Polarization and Dynamic Correlation in Singlet–Triplet Gap Inversion of Heptazine Derivatives, *J. Chem. Theory Comput.*, 2023, **19**, 7606–7616.